HHS Public Access

Author manuscript

Acta Biomater. Author manuscript; available in PMC 2016 April 15.

Published in final edited form as:

Acta Biomater. 2015 April 15; 17: 47–55. doi:10.1016/j.actbio.2015.01.022.

Phase stability and biological property evaluation of plasma sprayed hydroxyapatite coatings for orthopedic and dental applications

Sahar Vahabzadeh, **Mangal Roy**, **Amit Bandyopadhyay**, and **Susmita Bose***

W. M. Keck Biomedical Materials Research Laboratory School of Mechanical and Materials Engineering Washington State University Pullman, WA 99164, USA

Abstract

In this work we have investigated the effects of strontium (Sr) dopant on *in vitro* protein release kinetics and *in vivo* osteogenic properties of plasma sprayed hydroxyapatite (HA) coatings, along with their dissolution behavior. Plasma sprayed HA coatings are widely used in load-bearing implants. Apart from osseointegration, the new generation of HA coating is expected to deliver biomolecules and/or drugs that can induce osteoinduction. This paper reports the preparation of crystalline and amorphous HA coatings on commercially pure titanium (Cp-Ti) using inductively coupled radio frequency (RF) plasma spray, and their stability at different solution pH. Coatings prepared at 110 mm working distance from the nozzle showed average Ca ion release of 18 and 90 ppm in neutral and acidic environments, respectively. Decreasing the working distance to 90 mm resulted in the formation of a coating with less crystalline HA and phases with higher solubility products, and consequently higher dissolution over 32 days. A 92% release of a model protein bovine serum albumin (BSA) in phosphate buffer with pH of 7.4 was measured for Sr doped-HA coating, while only a 72% release could be measured for pure HA coating. Distortion of BSA during adsorption on coatings revealed strong interaction between the protein and the coating, with an increase in α-helix content. Osteoid formation was found on Sr-HA implants as early as 7 weeks post implantation compared to HA coated and uncoated Ti implants. After 12 weeks post implantation, osteoid new bone was formed on HA implants; whereas, bone mineralization started on Sr-HA samples. While no osteoid was formed on bare Ti surfaces, bone was completely mineralized on HA and Sr-HA coatings after 16 weeks post implantation. Our results show that both phase stability and chemistry can have significant influence towards *in vitro* and *in vivo* response of HA coatings on Ti implants.

Abstract

*Corresponding Author: Tel: 509 3357461; Fax: 509 3354662; sbose@wsu.edu.

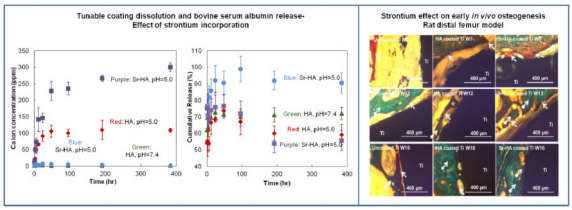

Keywords

Hydroxyapatite coating; induction plasma spray; load-bearing implants; dissolution behavior; *in vitro* protein release; denaturation; *in vivo* new bone formation

1. Introduction

Hydroxyapatite (HA, $Ca_{10}(PO_4)_6(OH)_2$) coated implants are being widely used to improve osteoconductivity of metallic implants [1,2]. In 2010, 719,000 total knee replacements (TKRs) and 332,000 total hip replacements (THRs) were performed only in the USA [3]. However, aseptic loosening, infection, instability and dislocation of implants result in >10% revisions in hip implants annually [4]. Since life expectancy is increasing and more implants are being placed in younger patients, the number of revision surgeries will also increase over time. Therefore, demand for new approaches to increase the life of load-bearing implants *in vivo* is ever increasing. We hypothesize that surface modification of titanium implants with doped hydroxyapatite enhances their stability and osteoconductivity, that will enhance implant lifetime *in vivo*.

Commercial HA coated implants are manufactured using a direct current (DC) plasma spray system due to ease of operation, low substrate temperature and low cost. However, plasma sprayed HA coatings often show secondary phases such as tricalcium phosphate (α/β form), calcium oxide (CaO), tetracalcium phosphate (TTCP) along with amorphous calcium phosphate (ACP) [5,6]. To achieve long term stability of a coating, the dissolution behavior of the coating is a critical factor. The two primary factors that control the dissolution characteristics of a coating are 1) inherent material properties such as chemical composition, presence of secondary phases, crystallinity, particle size, surface morphology, and roughness, and 2) environmental factors such as media composition and pH [5,6,7]. In HA coated implants, presence of ACP increases dissolution of coatings. Moreover, it has been reported that bone remodeling process generally results in a decrease of local pH to as low as 4 [8]. Therefore it is also important to understand the stability of HA coatings at and below the physiological pH, i.e., pH = 7.4. In this work, we have focused our attention to show the effects of plasma spraying parameters on crystallinity and physicochemical stability of HA coated implants at both neural and acidic environments and *in vivo* assessment using rat distal femur model.

Degradation of HA coating is expected on and around the coating surface during the biological fixation. This phenomenon of surface degradation can be utilized to locally deliver biomolecules such as bone morphogenic protein (BMP), bisphosphonate (BP) family of drugs, and angiogenic growth factors such as vascular endothelial growth factor (VEGF)

to facilitate bone regeneration *in vivo*. HA has been widely studied as a biomolecule carrier due to its high drug adsorption capability, biocompatibility, and pH dependent solubility [9,10]. Adsorption and release of several proteins and drugs such as bovine serum albumin (BSA), Vancomycin, Gentamicin and others have been studied using HA nanoparticles as a carrier [11,12].

In addition to pure HA, various trace elements such as strontium (Sr), magnesium (Mg), zinc (Zn), and silicon (Si) have been used as dopants in HA to enhance mechanical properties, improve crystallinity and control degradation / dissolution behavior [13,14,15]. Among them, Sr plays an important role on biomineralization of bone. Sr stimulates osteoblastic bone formation and also reduces bone resorption by osteoclasts [16,17]. Sr doped HA (Sr-HA) systems has also been used for delivery of drugs such as doxycycline hyclate and amoxicillin [18,19]. Therefore, we have used Sr-doped HA coatings to study the Sr effects on *in vitro* BSA release and *in vivo* new bone formation in rat distal femur model.

We hypothesize that coating chemistry and phase stability will influence the *in vitro* and *in vivo* responses of induction plasma sprayed coatings. To validate our hypothesis, in the present study we report the effects of plasma spraying parameters on physicochemical stability of HA coatings. We have investigated *in vitro* adsorption and release of BSA, a model protein, from HA and Sr-HA coatings at two different pH of 7.4 and 5.0. We have also studied the effects of HA and Sr-HA coatings on *in vivo* new bone formation in rat distal femur model over 16 weeks post implantation. Previously, we reported the effects of plasma spray manufacturing parameters, mainly plate power and working distance, on HA coating's phase composition and crystallinity [1]. In addition, we reported the effects of Sr dopant on phase composition, adhesive bond strength, and *in vitro* human fetal osteoblast (hFOB) cell-material interaction with plasma assisted hydroxyapatite coatings [13]. To the best of our knowledge, there is no report on investigation of Sr effects on *in vitro* BSA release and *in vivo* osteogenic properties of hydroxyapatite coatings prepared by induction plasma spray system.

2. Materials and Methods

2.1. Coating preparation

In our previous works, we have reported the preparation of pure and doped HA powders, as well as plasma sprayed coatings [1]. Briefly, commercial grade 150-212 μm sized HA powder (Monsanto, USA) was used to coat Ø 2.54cm X 2 mm commercially pure Ti disks (Grade 2, President Titanium, MA, USA). 1wt% Sr doped HA (Sr-HA) powder was prepared by ball milling of 50g HA with 0.60 g of SrO in 75 ml anhydrous ethanol for 6h. To achieve a proper particle size for plasma feed, ball milled powder was granulated at 800°C for 6h. Coatings were prepared using an inductively coupled RF plasma spray system (Tekna Plasma Systems, Canada-30 kW), attached with supersonic nozzle was used. HA coatings with three different crystallinity levels were prepared. Table 1 lists the plasma spray parameters used in the present work.

The HA and Sr-HA coatings for *in vitro* protein release and *in vivo* studies were prepared at plate power of 25 kW and 110 mm working distance. These parameters were selected from

previous optimization study where detail description about the supersonic plasma nozzle can also be found [1,13].

2.2. Microstructure and surface characterization

Top surface microstructural characterization of the coatings was performed using a field emission scanning electron microscope (FESEM, FEI 200F, FEI Inc., OR, USA). Different phases present in the coatings were determined by X-ray diffractometer (Siemens D500 Krystalloflex) using Cu Kα radiation at 35kV and 30 mA with a Ni-filter over the 2θ range between 20° and 50°, at a step size of 0.02° and a count time of 0.5 sec per step. Qualitative crystallinity of the HA phase in plasma sprayed coatings was determined as described in supplementary information. Fourier transform infrared (FTIR) spectra of samples were obtained using an ATR-FTIR spectrophotometer (Nicolet 6700 FTIR, Madison, WI, USA) in the 400 to 4000 cm^{-1} wave number range. Contact angles of different liquids on sintered HA and Sr-HA disk surfaces were measured using the sessile drop method. The liquid surface tension and their components were used to calculate surface energy as explained in supplementary information [20]. According to the ASTM F1926/F1926M-10 (standard test method for evaluation of the environmental stability of calcium phosphate granules, fabricated forms, and coatings), the dissolution experiments were done at pH 5.5 and pH 7.4 buffered media as explained in supplementary information.

2.3. In vitro BSA loading and release study

HA and Sr-HA coatings were used to study the release of BSA as a model protein. In order to investigate the BSA adsorption behavior, the coatings were immersed in 10 ml of BSA solution with the concentration of 6 mg/ml. They were kept at 36.5± 0.5 °C for 12h in an orbital shaker. Samples were then dried and the supernatant was collected to measure the amount of adsorbed BSA.

The release study was performed using phosphate buffer solution (PBS, pH= 7.4) and potassium hydrogen phthalate (PHT, pH=5.0) media. Each dried sample was put in a polypropylene vial containing 35 ml of medium, and incubated for 16 days at 36.5± 0.5 °C with continuous shaking at 150 rpm. The release amount of BSA was measured by collecting 600 μl of supernatant after 0.75, 1.5, 3, 6, 12, 24, 48, 96, 192, and 384h without further refilling. The BSA measurements in both steps (adsorption and release) were carried out using BCA protein assay kit (Pierce, Rockford, IL). Ti substrates were also used as the controlled sample during all steps. AAS was used to analyze Ca^{2+} concentration in the collected supernatant. Microstructural features of the coatings after release were also analyzed using FESEM at the accelerating voltage of 30kV.

Secondary structure of BSA was analyzed to investigate the protein denaturation after adsorption and release on HA and Sr-HA coatings. Gaussian curve fitting using the Origin software was performed on the protein amide I band region of FT-IR spectra. The area of assigned bands and the fraction of the total area in the region were calculated, which then presented as the fraction of α-helix and β-sheet subunits.

Ca^{2+} concentration, weight change, contact angle and surface energy, protein loading, *in vitro* release, and BSA secondary structure were analyzed in triplicates of samples. Measurements on each were also performed in three independent samples.

2.4. In Vivo study using a rat distal femur model

In this study, a total number of 18 male Sprague-Dawley rats (Simonsen Laboratories, Gilroy, CA, USA) with an average body weight of 300 g were used.

Surgeries were performed according to the approve protocol of Institutional Animal Care and Use Committee (IACUC) in Washington State University. Prior to surgery, rats were kept in humidity and temperature controlled room with alternating 12-hour cycles of dark and light. Anesthesia was performed using IsoFlo® (isoflurane, USP, Abbott Laboratories, North Chicago, IL, USA) coupled with an oxygen (Oxygen USP, A-L Compressed Gases Inc. , Spokane, WA, USA) regulator. After shaving and disinfection of skin, a longitudinal incision was made in distal region of the lateral aspect of the distal femur of all animals. Defects were created in the distal using drill at a slow rotation speed. To wash away the remaining bone fragments, the cavity was rinsed by physiological saline. Prior to implantation, all implants (3 × 3 × 5 mm) were sterilized at 121° C for 15 min. After implantation, muscle and skin were closed in layers using braided coated VICRYL (polyglactin 910) synthetic absorbable surgical suture (Ethicon Inc., Somerville, NJ, USA). To prevent infection, the wound site was cleaned with povidone iodine 5 % disinfectant. At 7, 12, and 16 weeks post-surgery, rats were euthanized by overdosing with halothane in a bell jar, followed by administration of an intracardiac injection of potassium chloride (70%).

Histomorphology and Masson Goldner's trichrome staining—All bone-implants for histological analysis were fixed in 10 % buffered formalin solution for 72 h. The specimens were then dehydrated in a graduated ethanol (70 %, 95 %, and 100 %), ethanol-acetone (1:1), and 100 % acetone series for undecalcified tissue sections preparation. After embedding samples in Spurr's resin, implant blocks were sectioned perpendicular to the implant axis using a low speed diamond saw. After polishing, the sections were stained by Masson Goldner's trichrome stain and observed under a light microscope [Olympus BH-2, Olympus America Inc., USA].

3. Results

3.1. In vitro dissolution of coatings

Figure 1 presents time and pH dependent release profile of Ca^{2+} during coating dissolution over 32 days. At pH 7.4, within the first 1.5 h, average Ca^{2+} release was 15 ppm, almost independent of coating type. With increase in time, 25-110 and 28-110 coatings did not show any further ion release and average Ca^{2+} concentration was 17 ppm at the end of 32 days (28-110 coating data is presented in Figure 2S). However, 28-90 sample showed a gradual increase in release with the final released ion concentration of ~49 ppm. Compared to neutral condition, Ca^{2+} release was time dependent for all coatings at pH 5.5. Similar to neutral pH, 25-110 and 28-110 samples did not have significant difference in ion release behavior and average Ca^{2+} concentration was 90 ppm after 32 days. The 28-90 sample

showed the highest initial ion release of 49 ppm, which increased up to ~137 ppm at 32 day time point.

3.2. HA and Sr-HA coatings: In vitro BSA adsorption and release behavior

Figure 2 shows presence of different phases in HA and Sr-HA coatings. HA was the major phase in both coatings. Small amounts of β-TCP and α-TCP were also found in these coatings; however, there was no undesirable phase such as TTCP or CaO. HA and Sr-HA disk samples had 58.18±4.90° and 55.20±3.38° contact angles with water, respectively. HA sample had a surface energy of 71.25 mJ/m^2, whereas surface energy of Sr-HA was 119.87 mJ/m^2. UV-Vis spectroscopy was used to determine the loaded BSA amount on HA and Sr-HA coatings. A total of 360 and 490 μg of BSA was successfully loaded on HA and Sr-HA coatings, respectively after 12 h of immersion in BSA solution. It is worth to mention that in current study, coatings were kept in BSA solution for 6, 12, and 24 h, and 12 h time point was found as the equilibrium time for BSA adsorption. The FT-IR spectra of BSA, HA and Sr-HA coatings are presented in Figure 3. Both coatings showed the characteristic bands of PO_4^{3-} In addition, BSA amide-I, amide-II and amide-III bands were present in coatings spectra after BSA loading (Figures 3c and e).

In vitro BSA release was performed in PBS and PHT buffer solutions with pH of 7.4 and 5.0, respectively and results are presented in Figure 4. Initial BSA burst release was noticed for HA and Sr-HA coatings at both pH 7.4 and 5.0. At pH 7.4, BSA released amount reached ~ 72% and 92% for HA and Sr-HA coatings, respectively, at the end of 24 h, followed by insignificant change in protein release until the end of experiment. At pH 5.0, both HA and Sr-HA coatings showed similar release trend. BSA release reached a maximum of ~74% and 76% at 48 h, followed by a significant drop of 59% and 54% for HA and Sr-HA coatings, respectively at 192 h. No further change in release amount was observed at pH 5.0.

Table 2 shows the secondary structure analysis of pure BSA, BSA loaded on HA and Sr-HA coatings, as well as the released BSA after 7 days from both coatings. The α-helix content determined from FT-IR spectra in the amide I region was 22±1 and 27±1 % after adsorption on HA and Sr-HA coatings, respectively. The α-helix amount in released BSA from HA and Sr-HA coatings after 7 days increased to 30±1 and 32±1 %, respectively.

3.3. Dissolution of BSA loaded HA and Sr-HA coatings

HA and Sr-HA coatings showed 72.5 and 64.3 % crystallinity, respectively. To evaluate the pH effect on dissolution of BSA loaded HA and Sr-HA coatings, Ca^{2+} concentration was determined using AAS. Figure 5 shows pH and coating chemistry effects on dissolution characteristics of HA and Sr-HA coatings. At pH 7.4, no significant dissolution occurred. However, at pH 5.0, Ca^{2+} concentration increased up to 106 ppm for HA coating at 48h and then remained constant. Sr-HA coating showed the burst dissolution with Ca^{2+} concentration of 228 ppm at 48 h, followed by a gradual disintegration of coating. The maximum concentration of Ca^{2+} was 300 ppm at 384h for Sr-HA coating.

Figure 6 shows the FESEM images of coatings after BSA release for both pH of 5.0 and 7.4. Although there were no significant changes on coatings at pH 7.4, acidic pH caused crack formation on both types of samples due to faster dissolution of coatings.

3.4. In vivo studies: Histomorphology

To understand the effects of Sr addition on new bone formation, histological evaluations were performed at 7, 12, and 16 weeks and results are shown in Figures 7 **and** 8. At 7 weeks, uncoated Ti showed a large gap between the implant and the newly forming osteoid (colored in red) which was significantly lower for HA coating. A substantial difference was noticed in Sr-HA sample at 7 weeks showing osteoid formation on the implant surface which was not started on either Ti or HA coated Ti. At 12 weeks, bone started to mineralize on Sr-HA coated implant surface which was not present on uncoated Ti and HA coated implant. Unlike uncoated Ti, osteoid formation was prominent on HA coating indicating accelerated bone regeneration in HA coatings compared to uncoated Ti implants. However, new bone formation was slower on HA coatings in comparison to Sr-HA coated implants, as shown in Figure 7. With progress in time, complete bone mineralization was found on and around HA and Sr-HA coated implants showing little difference between them after 16 weeks post implantation. As expected, no osteoid formation was noticed on the uncoated Ti surface. However, the gap between the host bone and implant surface was reduced indicating movement of the host bone front towards the uncoated Ti surface, as presented in Figure 8.

4. Discussion

Dissolution behavior is an important factor which determines coating functionality of a coated medical device in orthopedic applications. Chemistry of coating, particle size, crystallinity, and the dissolution media properties such as chemistry and pH are the most crucial parameters which affect coating dissolution [21]. We have already reported the effects of plasma spraying parameters on microstructure and surface characterization of HA coatings [1]. In this study, dissolution behavior of HA coatings with different crystallinity levels, achieved by various plate power and working distance, was studied in acidic and neutral buffer media. The scientific understanding is further used to investigate the effects of coating composition on *in vitro* protein release kinetics and *in vivo* osteogenesis in rat distal femur model.

As shown in Figure 1S, 25-110 and 28-110 coatings include HA as major phase with small amount of α-TCP and β-TCP. However, increasing the power from 25 kW to 28 kW in 110 mm working distance is accompanied by decrease in crystalline HA phase from 72.5% to 60.2%, due to higher melting of particles as applied plate power increases. In 28-90 coating; however, decomposition of HA to α-TCP and β-TCP, as well as TTCP phase formation are accelerated due to higher plasma-HA secondary and prolonged interaction at very short 90 mm working distance [1].

HA coating degradation is generally governed by either osteoclast mediated cellular resorption or chemical degradation. Degradation of HA coatings also results in initiation of another competing process, reprecipitaion of apatite layer. The dynamics between

dissolution and precipitation govern the long-term use of coatings. Dissolution of coatings is controlled by crystallinity, presence of secondary phases, porosity in the coating, and solution pH whereas their precipitation is dominated by ion concentration [5,22]. At pH 5.5, high dissolution of coatings along with the absence of precipitation results in weight loss for all three coatings, as shown in Figures 2S-4S. In acidic pH, coating dissolution depends on solubility isotherm, particle size, surface area and coating crystallinity [23]. In the present study, chemistry and HA phase crystallinity of coatings are dominant factors affecting their dissolution. 28-90 coating show significant weight loss compared to coatings with 60% and 72% crystallinity, due to the presence of phases with higher solubility product and higher amorphous phase content. Direct dissolution dependency on crystallinity at pH 7.4 is also found in our work which is in line with literature [23]. In addition, our results show that the precipitation is the dominant process at pH 7.4. Precipitation occurrence is in line with results found by Sun *et al.* [6]. 28-90 sample show the highest dissolution rate with plate-like particle formation. To retain HA phase purity, crystallinity and low dissolution rate, the power of 25 kW and nozzle-sample distance of 110 mm is selected for further study. These parameters lead to formation of HA and Sr-HA coatings with thickness of 312 ± 34μm and 317 ± 56μm, respectively [13].

BSA adsorption was performed at neutral condition. Isoelectric point of BSA is 4.7, and protein interacts with coatings through electrostatic interaction between COO- and present cations in HA and Sr-HA coatings [24,25]. Regardless of coating roughness, higher protein adsorption on Sr-HA sample is due to higher surface energy of Sr-HA. The FT-IR spectra of BSA loaded HA and Sr-HA coatings in Figure 3c and e confirms the presence of BSA in these two samples. In addition, as shown in Figure 5S, surface morphology of HA and Sr-HA coatings does not change due to BSA adsorption.

Protein release studies show the burst release of BSA in early time points, regardless of coating chemistry and media pH. The initial high release of drugs and proteins from calcium phosphate structures has already been reported by others [18,25,26]. Although higher release of protein/drug is reported due to higher dissolution rate of coatings in acidic pH [24], the present study shows that there is a significant decrease in release at lower pH. In addition, after reaching the maximum, both coatings show a significant drop in protein release. Although there are different trends in release regarding the media pH and coating chemistry, all samples reach the equilibrium within 192 h. Figure 5 shows higher Ca^{2+} concentration at pH 5.0 due to higher dissolution in acidic pH, accompanied by crack formation on coating surface revealed by SEM, as shown in Figure 6. The difference in release kinetics from coating and particle system could be due to the difference in surface area between the two systems. In a particulate system, protein or other molecules are adsorbed (physisorbed or chemisorbed) on each particle with higher surface area compared to the coatings [24,27], as a result, higher released amount is expected with faster dissolution rate. In coatings, however, loading is performed only on the free particles of surface. As dissolution of top layer occurs, new bare particles on surface are exposed to BSA saturated media. We hypothesize that protein is re-adsorbed in this condition, which is not expected in particulate system. Figure 9 shows the described mechanism schematically. Figure 9a represents the as-loaded coating. During the release period, some cracks are formed on the coating, as shown

in Figure 9b. In this step, dissolution of coating and BSA release are the dominant processes. However, at later time points, the release and readsorption of the BSA reaches the equilibrium. It is worth noting that the BSA readsorption might be due to lack of media flow. Under dynamic condition, although the dissolution occurs, readsorption can be insignificant due to presence of concentration gradient between the sample and the medium [28].

Both media pH and coating chemistry have significant effect on BSA release. BSA release amount from Sr-HA coatings are higher than pure HA coatings at neutral pH, while lower BSA release is noticed in acidic conditions from Sr-HA coating. These changes in release behavior are related to coating dissolution and crystallinity. Higher dissolution of Sr-HA coating at both pH 5.0 and 7.4 is directly related to its lower crystallinity. Although increase in the HA crystallinity by Sr addition at high level of doping is reported elsewhere [19], our results are in accordance with Zhang *et al.* who reported the lower crystallinity of Sr-HA compounds due to structural strain during Sr ionic substitution in Ca sites [17]. At neutral pH, higher BSA is released from Sr-HA coatings due to faster dissolution. However, based on readsorption of protein in acidic solution, more significant drop in release plot is expected for doped coatings due to their lower crystallinity.

BSA secondary structure was analyzed using Gaussian curve fitting under IR spectrum in the amide I IR band (1600-1700 cm-1). Decrease in α-helix content after BSA adsorption is due to strong electrostatic interaction between the coating and the BSA. However, increase in α-helix content after 7 days of release shows relaxation of electrostatic interactions by protein detachment from coatings [25].

To evaluate the effects of HA and Sr-HA coatings on *in vivo* osteogenesis of Ti implant, histological analysis was performed after 7, 12, and 16 weeks post implantation. As shown in Figure 7, presence of Sr accelerates the bone formation on the implant surface. During implant integration, bridging the gap between host bone surface and implant surface dictates the recovery time. The recovery time is minimal when osteogenesis occurs at both the implant surface and host bone. In case of Sr-HA coated implants, osteoid formation starts by week 7 on the implant surface which is not present on either uncoated or HA coated Ti implants. These results are well supported by *in vitro* and *in vivo* investigations. Sr has stimulatory effect on osteoblast cell proliferation and differentiation through activation of parallel calcium sensing pathways and *cbfa1* gene, and leads to early osteoid formation [13,29,30,31]. It also results in higher expression of alkaline phosphatase (ALP) and osteocalcin (OC) [32]. In addition, Sr leads to osteoclast cell apoptosis and inhibits osteoclastogenesis [29,33]. In Sr-HA system, Sr induces bone formation by enhancing dissolution-reprecipitation mechanism. Presence of Sr increases the degradation rate, as shown in Figure 5, and results in higher concentration of calcium, phosphate, and strontium ions. Subsequently, the reprecipitation of apatite in presence of collagen occurs which in turn enhances the protein absorbance and osteoblast cell adhesion and proliferation [34,35,36]. With time, bone regeneration also starts on HA coated Ti. As shown in Figure 8, there is no significant difference in bone mineralization between HA and Sr-HA coatings after 16 weeks post implantation. Therefore, it is concluded from the present *in vivo* results that presence of Sr allows early osteogenesis on HA coated implant surface. Thus, HA and

Sr-HA plasma coated Ti implants have great potential for delivery of biomolecules and early osteogenesis in bone tissue engineering applications.

Conclusions

Here we report crystallinity and environmental effects on stability of plasma sprayed HA coatings. Coating prepared at 90 mm distance of substrate from nozzle was composed of α-TCP, β-TCP, TTCP, and HA with 45% crystallinity. Increase in the distance resulted in formation of coatings with higher crystallinity. Coating stability was severely compromised by crystallinity in both neutral and acidic environments. Coating prepared at plate power of 28 kW and 90 mm standoff distance, had the Ca^{2+} release of 49 and 137 ppm in neutral and acidic conditions, respectively, which was the highest release compared to coatings prepare at lower plate power and/or higher distance. To retain HA phase purity and crystalliniy, HA and Sr-HA coatings were prepared at 25 kW plate power and 110 mm standoff distance, to study the effect of coating chemistry on BSA release behavior. Sr addition resulted in formation of structure with lower crystallinity, and thus higher dissolution of coating, releasing 92% of BSA in neutral condition. Both HA and Sr-HA coatings showed higher dissolution rate in acidic condition, however, due to protein readsorption, lower BSA concentration was measured at this pH. After 7 weeks post implantation, osteoid was formed on Sr-HA compared to HA coated and uncoated Ti implants. Osteoid formation was found on HA implant after 12 weeks post implantation; whereas, bone mineralization started on Sr-HA samples at this time point. While no osteoid was formed on bare Ti surfaces, bone was completely mineralized on HA and Sr-HA coatings after 16 weeks post implantation. These results show the effects of plasma spraying parameters and coating composition on crystallinity, dissolution, protein release behavior, and *in vivo* bone regeneration which can be tailored to meet specific clinical application needs.

Supplementary Material

Refer to Web version on PubMed Central for supplementary material.

Acknowledgements

Authors would like to acknowledge financial support from the National Institutes of Health, (Grant # NIH 1R01AR066361 and NIH 1R01EB007351). The authors wish to also acknowledge the School of Mechanical and Materials Engineering as well as the Franceschi Microscopy & Imaging Center.

References

1. Roy M, Bandyopadhyay A, Bose S. Induction plasma sprayed nano hydroxyapatite coatings on titanium for orthopaedic and dental implants. Surf Coat Technol. 2011; 205:2785–2792. [PubMed: 21552358]
2. Bandyopadhyay, A.; Bose, S. Characterization of biomaterials. 1st ed. Elsevier Publication; 2013.
3. http://www.cdc.gov/nchs/fastats/insurg.htm
4. Springer BD, Fehring TK, Griffin WL, Odum SM, Masonis JL. Why revision total hip arthroplasty fails. Clin Orthop Relat Res. 2009; 467:166–173. [PubMed: 18975043]
5. Zhang Q, Chen J, Feng J, Cao Y, Deng C, Zhang X. Dissolution and mineralization behaviors of HA coatings. Biomaterials. 2003; 24:4741–4748. [PubMed: 14530071]

6. Sun L, Berndt CC, Khor KA, Cheang HN, Gross KA. Surface characteristics and dissolution behavior of plasma-sprayed hydroxyapatite coating. J Biomed Mater Res. 2002; 62:228–236. [PubMed: 12209943]
7. Kweh SW, Khor KA, Cheang P. An in vitro investigation of plasma sprayed hydroxyapatite (HA) coatings produced with flame-spheroidized feedstock. Biomaterials. 2002; 23:775–785. [PubMed: 11774849]
8. Teti A, Blair HC, Schlesinger P, Grano M, Zambonin-Zallone A, Kahn AJ, Teitelbaum AJ, Hruska KA. Extracellular protons acidify osteoclasts, reduce cytosolic calcium, and promote expression of cell-matrix attachment structures. J Clin Invest. 1989; 84:773–780. [PubMed: 2547838]
9. Bose S, Tarafder S. Calcium phosphate ceramic systems in growth factor and drug delivery for bone tissue engineering: A review. Acta Biomater. 2012; 8:1401–1421. [PubMed: 22127225]
10. Yang P, Quan Z, Li C, Kang X, Lian H, Lin J. Bioactive, luminescent and mesoporous europium-doped hydroxyapatite as a drug carrier. Biomaterials. 2008; 29:4341–4347. [PubMed: 18715638]
11. Stigter M, Bezemer J, de Groot K, Layrolle P. Incorporation of different antibiotics into carbonated hydroxyapatite coatings on titanium implants, release and antibiotic efficacy. J. Controlled Release. 2004; 99:127–137.
12. Dasgupta S, Banerjee SS, Bandyopadhyay A, Bose S. Zn- and Mg-doped hydroxyapatite Nanoparticles for Controlled Release of Protein. Langmuir. 2010; 26:4958–4964. [PubMed: 20131882]
13. Roy M, Bandyopadhyay A, Bose S. Induction plasma sprayed Sr and Mg doped nano hydroxyapatite coatings on Ti for bone implant. J Biomed Mater Res Part B. 2011; 99B:258–265.
14. Bandyopadhyay A, Bernard S, Xue W, Bose S. Calcium phosphate-based resorbable ceramics: influence of MgO, ZnO, and SiO_2 dopants. J Am Ceram Soc. 2006; 89:2675–2688.
15. Banerjee SS, Tarafder S, Davies NM, Bandyopadhyay A, Bose S. Understanding the influence of MgO and SrO binary doping on the mechanical and biological properties of β-TCP ceramics. Acta Biomater. 2010; 6:4167–4174. [PubMed: 20493283]
16. Xue W, Moore JL, Hosick HL, Bose S, Bandyopadhyay A, Lu WW, Cheung KM, Luk KD. Osteoprecursor cell response to strontium-containing hydroxyapatite ceramics. J Biomed Mater. Res Part A. 2006; 79A:804–814.
17. Zhang W, Shen Y, Pan H, Lin K, Liu X, Darvell BW, Lu WW, Chang J, Deng L, Wang D, Huang W. Effects of strontium in modified biomaterials. Acta Biomater. 2011; 7:800–808. [PubMed: 20826233]
18. Alkhraisat MH, Rueda C, Cabrejos-Azama J, Lucas-Aparicio J, Mariño FT, Torres García-Denche J, Jerez LB, Gbureck U, Cabarcos EL. Loading and release of doxycycline hyclate from strontium-substituted calcium phosphate cement. Acta Biomater. 2010; 6:1522–1528. [PubMed: 19879982]
19. Suganthi RV, Elayaraja K, Joshy MIA, Chandra VS, Girija EK, Kalkura SN. Fibrous growth of strontium substituted hydroxyapatite and its drug release. Mater Sci Eng C. 2011; 31:593–599.
20. Van Oss CJ, Giese RF Jr, Good RJ. Reevaluation of the surface tension components and parameters of polyacetylene from contact angles of liquids. Langmuir. 1990; 6:1711–1713.
21. Surmenev RA, Surmeneva MA, Ivanova AA. Significance of calcium phosphate coatings for the enhancement of new bone osteogenesis – A review. Acta Biomater. 2014; 10:557–579. [PubMed: 24211734]
22. Mohammadi Z, Ziaei-Moayyed AA, Sheikh-Mehdi Mesgar A. In vitro dissolution of plasma-sprayed hydroxyapatite coatings with different characteristics: experimental study and modeling. Biomed Mater. 2008; 3 DOI:10.1088/1748-6041/3/1/015006.
23. Wang J, Layrolle P, Stigter M, de Groot K. Biomimetic and electrolytic calcium phosphate coatings on titanium alloy: physicochemical characteristics and cell attachment. Biomaterials. 2004; 25:583–592. [PubMed: 14607496]
24. Dasgupta S, Bandyopadhyay A, Bose S. Reverse micelle-mediated synthesis of calcium phosphate nanocarriers for controlled release of bovine serum albumin. Acta Biomater. 2009; 5:3112–3121. [PubMed: 19435617]
25. Tarafder S, Banerjee S, Bandyopadhyay A, Bose S. Electrically polarized biphasic calcium phosphates: adsorption and release of bovine serum albumin. Langmuir. 2010; 26:16625–16629. [PubMed: 20939493]

26. Zhang C, Li C, Huang S, Hou Z, Cheng Z, Yang P, et al. Self-activated luminescent and mesoporous strontium hydroxyapatite nanorods for drug delivery. Biomaterials. 2010; 31:3374–3383. [PubMed: 20122726]
27. Vahabzadeh S, Edgington J, Bose S. Tricalcium phosphate and tricalcium phosphate/polycaprolactone particulate composite for controlled release of protein. Mater Sci Eng C. 2013; 33:3576–3582.
28. Gbureck U, Vorndran E, Barralet JE. Modeling vancomycin release kinetics from microporous calcium phosphate ceramics comparing static and dynamic immersion conditions. Acta Biomater. 2008; 4:1480–1486. [PubMed: 18485844]
29. Yang L, Perez-Amodio S, Barrere-de Groot FYF, Everts V, Blitters- wijk CAV, Habibovic P. The effects of inorganic additives to calcium phosphate on in vitro behavior of osteoblasts and osteoclasts. Biomaterials. 2010; 31:2976–2989. [PubMed: 20122718]
30. Sila-Asna M, Bunyaratvej A, Maeda S, Kitaguchi H, Bunyaratavej N. Osteoblast differentiation and bone formation gene expression in strontium-inducing bone marrow mesenchymal stem cell. Kobe J Med Sci. 2007; 53:25–35. [PubMed: 17579299]
31. Tat SK, Pelletier JP, Mineau F, Caron J, Martel-Pelletier J. Strontium ranelate inhibits key factors affecting bone remodeling in human osteoarthritic subchondral bone osteoblasts. Bone. 2011; 49:559–567. [PubMed: 21700005]
32. Bonnelye E, Chabadel A, Saltel F, Jurdic P. Dual effect of strontium ranelate: stimulation of osteoblast differentiation and inhibition of osteoclast formation and resorption in vitro. Bone. 2008; 42:129–38. [PubMed: 17945546]
33. Saidak Z, Marie PJ. Strontium signaling: molecular mechanisms and therapeutic implications in osteoporosis. Pharmacol Ther. 2012; 136:216–226. [PubMed: 22820094]
34. Ni GX, Lu WW, Xu B, Chiu KY, Yang C, Li ZY, Lam WM, Luk KD. Interfacial behaviour of strontium-containing hydroxyapatite cement with cancellous and cortical bone. Biomaterials. 2006; 27:5127–5133. [PubMed: 16781769]
35. Chen QZ, Wong CT, Lu WW, Cheung KMC, Leong JCY, Luk KDY. Strengthening mechanisms of bone bonding to crystalline hydroxyapatite in vivo. Biomaterials. 2004; 25:4243–4254. [PubMed: 15046914]
36. Wang J, Zhang L, Sun X, Chen X, Xie K, Lin M, Yang G, Xu S, Xia W, Gou Z. Preparation and in vitro evaluation of strontium-doped calcium silicate/gypsum bioactive bone cement. Biomed Mater. 2014; 9 DOI:10.1088/1748-6041/9/4/045002.

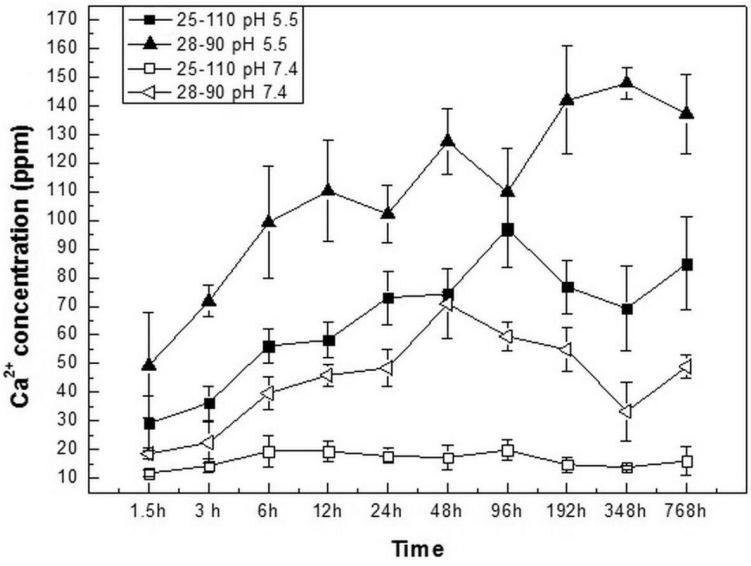

Figure 1.

Ca^{2+} concentration in buffer media during dissolution from 25-110 and 28-90 coatings.

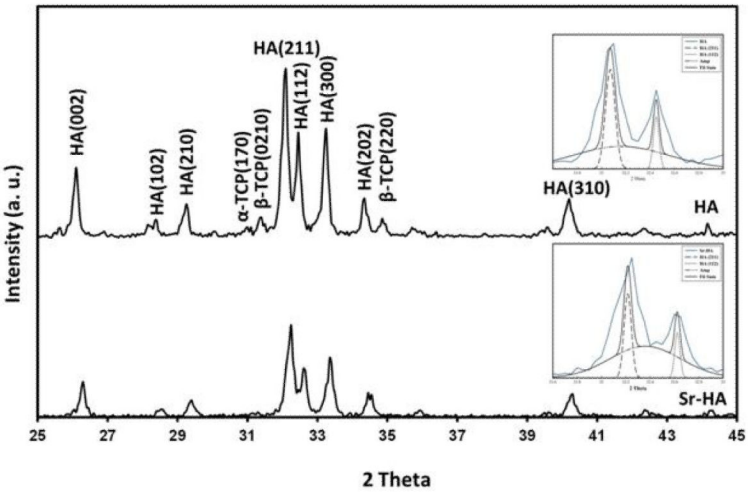

Figure 2.
XRD pattern of HA and Sr-HA coatings prepared by plasma spray.

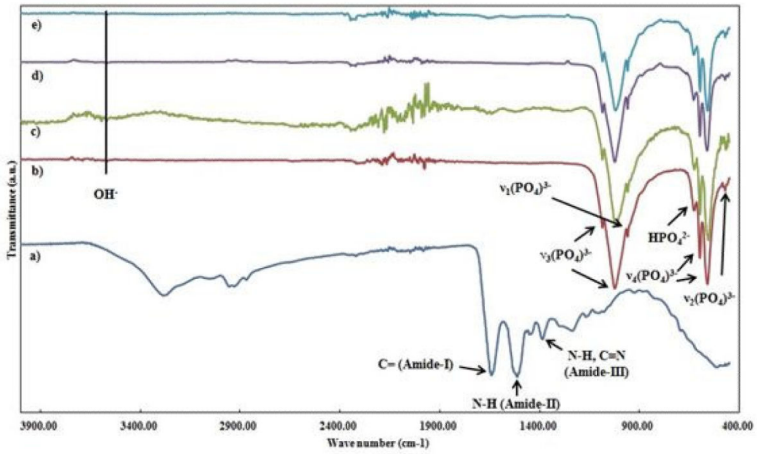

Figure 3.

The FT-IR spectra of a) BSA, b) as prepared HA, c) BSA loaded HA, d) as prepared Sr-HA, and e) BSA loaded Sr-HA coatings.

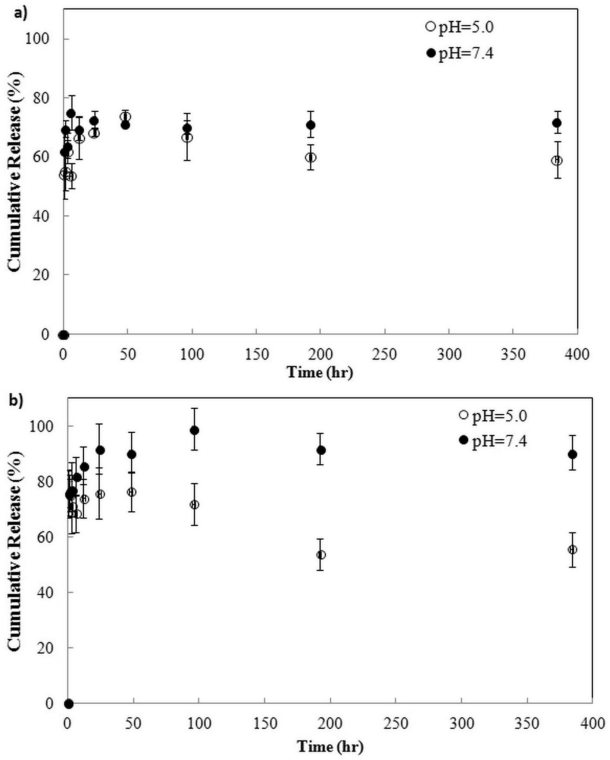

Figure 4.
BSA release plot from the a) HA and b) Sr-HA coatings.

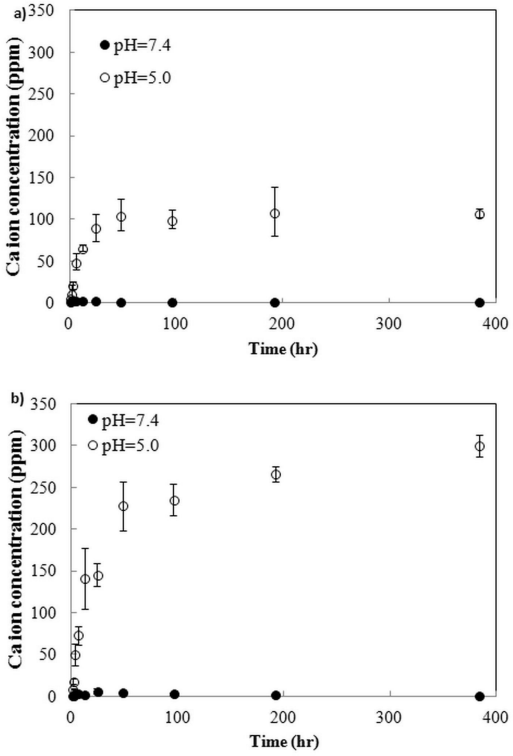

Figure 5.

Ca^{2+} concentration in buffer media during the release from coatings of, a) HA and b) Sr-HA.

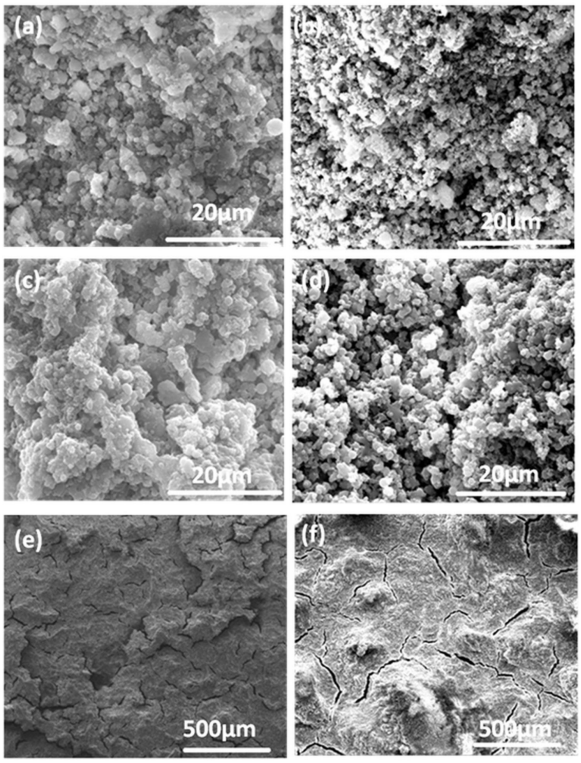

Figure 6.

FESEM micrographs of coatings after release; a) HA at pH=7.4, b) Sr-HA at pH=7.4, c) HA at pH=5.0, d) Sr-HA at pH=5.0. (e) and f) are lower magnification images of HA and Sr-HA at pH=5.0.

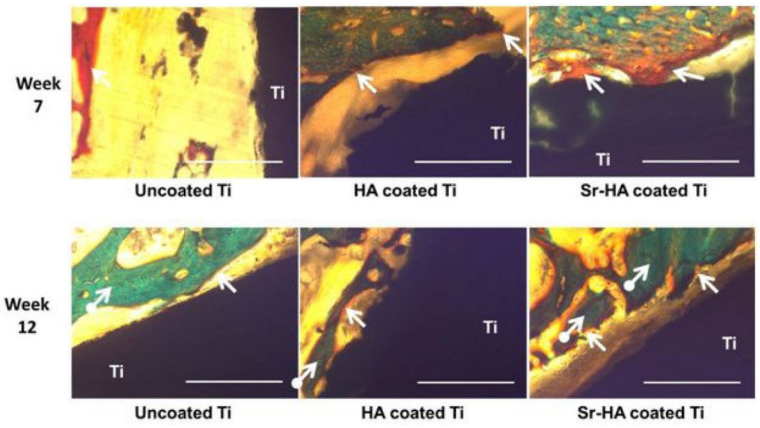

Figure 7.

Optical photomicrograph of a longitudinal section of uncoated Ti, HA coated Ti, and Sr-HA coated Ti implants showing the development of new bone formation on the surface of implants after 7 and 12. Modified Masson Goldner's trichrome staining of transverse section. Color descrition: orange/red = nonmineralized osteoid (indicated by arrow), green = mineralized bone (indicated by circled arrow). The scale bar represents 400μm.

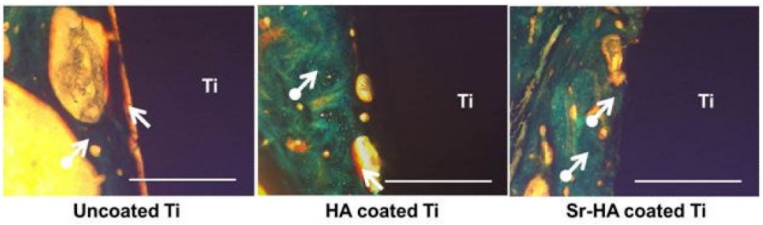

Figure 8.

Optical photomicrograph of a longitudinal section of uncoated Ti, HA coated Ti, and Sr-HA coated Ti implants showing the development of new bone formation on the surface of implants after 16 weeks. The scale bar represents 400μm.

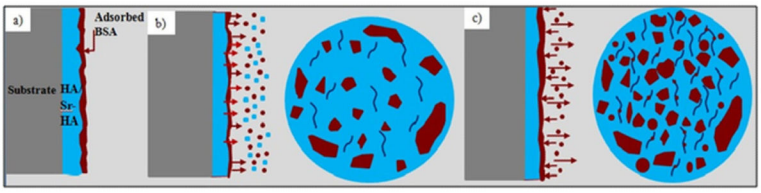

Figure 9.
Coating surface during release steps: a) at the beginning, b) in the middle, and c) at the end.

Table 1

Plasma spray coating variables for samples.

Sample	Power (kW)	Nozzle-sample distance (mm)	% Crystallinity of HA phase
25-110	25	110	72.5
28-110	28	110	60.2
28-90	28	90	45.6

Table 2

Secondary structure of pure, loaded, and released BSA.

Sample	α-helix (±1%)	β-sheet (±1%)
Pure BSA	38.00	41.00
BSA loaded on HA coating	22.00	44.00
BSA loaded on Sr-HA coating	27.00	48.00
BSA released from HA coating, after 7days	30.00	37.00
BSA released from Sr-HA coating, after 7days	32.00	37.00